ELSEVIER

Mathematical Biosciences 161 (1999) 15–41

Mathematical Biosciences
an international journal

www.elsevier.com/locate/mathbio

A new analytical method of studying post-synaptic currents

D.S. Poskitt [a], K. Doğançay [b], Shin-Ho Chung [b,*]

[a] *Department of Statistics, Australian National University, Canberra, ACT 0200, Australia*
[b] *Department of Chemistry, Australian National University, Canberra, ACT 0200, Australia*

Received 25 September 1998; received in revised form 3 June 1999; accepted 14 July 1999

Abstract

A powerful methodology for analyzing post-synaptic currents recorded from central neurons is presented. An unknown quantity of transmitter molecules released from presynaptic terminals by electrical stimulation of nerve fibers generates a post-synaptic response at the synaptic site. The current induced at the synaptic junction is assumed to rise rapidly and decay slowly with its peak amplitude being proportional to the number of released transmitter molecules. The signal so generated is then distorted by the cable properties of the dendrite, modeled as a time-invariant, linear filter with unknown parameters. The response recorded from the cell body of the neuron following the electrical stimulation is contaminated by zero-mean, white, Gaussian noise. The parameters of the signal are then evaluated from the observation sequence using a quasi-profile likelihood estimation procedure. These parameter values are then employed to deconvolve each measured post-synaptic response to produce an optimal estimate of the transmembrane current flux. From these estimates we derive the amplitude of the synaptic current and the relative amount of transmitter molecules that elicited each response. The underlying amplitude fluctuations in the entire data sequence are investigated using a non-parametric technique based on kernel smoothing procedures. The effectiveness of the new methodology is illustrated in various simulation examples.

Keywords: Post-synaptic currents; Quantal analysis; Amplitude histogram deconvolution; Blind deconvolution; Kernel smoothing; Model of synaptic currents

* Corresponding author. Tel.: +61-2 6249 2024; fax: +61-2 6247 2792; e-mail: shin-ho.chung@anu.edu.au

0025-5564/99/$ - see front matter
PII: S0025-5564(99)00038-3

1. Introduction

The analysis of post-synaptic currents recorded from neurons has, hitherto, commonly proceeded along the following lines. Because of the physical dimensions of the dendrite the measurement of the current that flows through the ion channels in the membrane is generally made at the cell body. The amplitude of each evoked response is estimated from the observed current by examining the magnitude of the evoked response, relative to a baseline, in a small neighborhood of the peak current. In essence a narrow width time averaging window is applied. From the amplitude estimates so obtained an amplitude histogram is constructed. This histogram is assumed to be generated from a realization of independent and identically distributed data values taken from a finite mixture distribution and so the histogram is then deconvolved into a number of underlying component parts [1–7]. The primary aim of such an analysis has been to infer the number and structure of the underlying distributions that give rise to the observed amplitude histogram. [1]

Unfortunately, the application of this conventional technique to currents recorded from neurons in the central nervous system can be severely hampered by low signal-to-noise ratios. Since the measurements are made some distance away from the synaptic site it seems likely that the original signal will be attenuated, having had its shape distorted by the cable properties of the dendrite, and the recording will obviously be contaminated by various sources of noise. Thus it is desirable to have an alternative data processing scheme which allows the magnitude of the noise obscuring the observed signal to be drastically increased whilst still enabling accurate estimates of the signal profile and the peak amplitude to be evaluated. Once reliable estimates of these are obtained, many questions of fundamental theoretical importance relating to the mechanism underlying synaptic transmission can then be more readily resolved. For example, whether or not the release of transmitter molecules occurs in quanta, the magnitude of the quantal variation, if any, and determination of the number of release sites on the dendritic segments. Such an analysis might also reveal if the magnitude of the neurotransmitter release increases following the induction of long-term potentiation [9]. Also, from the estimated shape of the signals of differing amplitudes, it may be possible to deduce the location of the synaptic sites relative to the cell body from which the recording is made.

We present here a novel method of analyzing post-synaptic currents whose realization is embedded in noise. The current generated by the released neurotransmitter at the synaptic site is assumed to rise rapidly and then decay monotonically. The response recorded at the cell body will, however, be distorted by the filtering properties of the dendritic segment. Thus, the observed

[1] Note that not all procedures are based on an examination of the histogram, see [8] for example.

process is construed as being the output from a time-invariant linear filter driven by an impulse, representing the evoked release of neurotransmitter, to which zero-mean, white Gaussian noise is added. We further assume that the signal arriving at the neuronal cell body can be delayed for various durations after stimulation of the afferent fiber. Our model allows us to estimate the unknown parameters that characterize the filter as well as the amplitude of the post-synaptic current embedded in each segment of the record. From these estimates, other relevant statistics, such as the amplitude histogram, the number of release sites, quantal content and coefficient of variation, can be deduced. First we describe the methodology at an intuitive level and then, using simulated data designed to mimic post-synaptic currents embedded in noise, we demonstrate that the analytical scheme we propose can identify the process parameters with acceptable accuracy.

2. Theoretical background

2.1. Signal model

Consider a discrete-time stochastic process $\{y(k)\}$,

$$y(k) = s(k) + \eta(k), \quad k = 0, 1, \ldots, T-1, \tag{1}$$

which represents the observed measurements, consisting of the underlying signal $\{s(k)\}$ at the recording site and the measurement noise $\{\eta(k)\}$, made on the evoked post-synaptic current records over the interval $[0, T-1]$. The afferent nerve fibers are assumed to be stimulated at regular intervals L time periods apart and, after a brief conduction delay, packets of neurotransmitter molecules are released from axonal terminals generating a pulse. We model the observations as the noise corrupted output of a linear time-invariant system that is being driven by an input $u(k)$ composed of a periodic pulse train where the time interval between pulses, L, is given but the amplitude of each pulse, $\{a(i)\}$, is an independent and identically distributed sequence of random variables drawn from a probability distribution $\mathbb{P}_A$ with $a(i) \geqslant 0$. This is illustrated schematically in Fig. 1. Here the pulse height $a(i)$, which is not directly observable, represents the quantity of released transmitter molecules. Each of these pulses is then assumed to be transformed into a post-synaptic current according to some transfer function $P(z)$ but the shape of the current becomes distorted by the cable properties of the dendrite, which we represent as a low-pass filter $F(z)$. Thus, the measurements $\{y(k)\}$ in our model are related to the impulse response sequence $\{c(i),\ i \geqslant 0\}$ of the overall transfer function $C(z) = \sum_{i \geqslant 0} c(i) z^{-i}$ and the input sequence $\{u(k)\}$ via $y(k) = c * u(k) + n(k)$ where $c * u(k)$ denotes the convolution of the impulse response sequence and the input process at time point k and $n(k)$ denotes the residual.

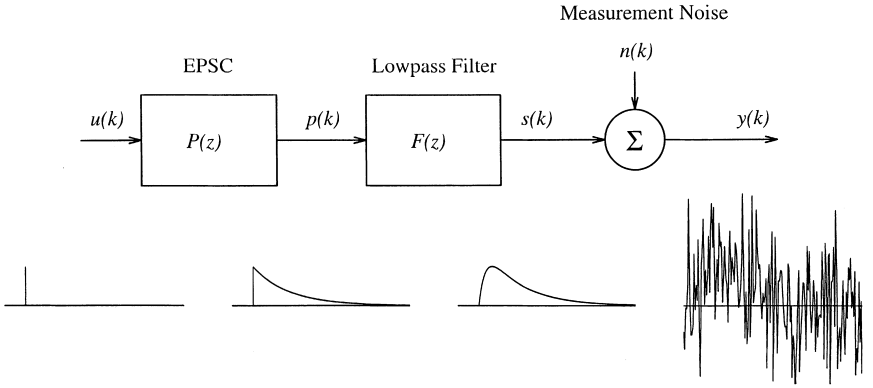

Fig. 1. The signal model. Transmitter molecules $u(k)$ released from presynaptic terminals, indicated here as vertical lines whose heights are proportional to the number of released molecules, evoke post-synaptic currents recorded from the cell body. The currents at the synaptic site are assumed to rise instantaneously and decay exponentially, as indicated by the first transfer function, $P(z)$. As the signal is spread down electrotonically to the cell body its shape becomes distorted by the cable properties of the dendrite and this distortion is characterized by the second transfer function, $F(z)$. To this signal is added the zero-mean, white Gaussian noise $n(k)$ to give the measured response $y(k)$.

The residual process $\{n(k)\}$ captures such features as the measurement error and the discrepancy between $c * u(k)$ and the true $s(k)$, the modeling error. In technical parlance, $C(z)$ is given by a stable and causal system of the form

$$C_\alpha(z) = \alpha_0 \prod_{i=0}^{p-1} (1 - \xi_i z)^{-1} \tag{2a}$$

$$= \alpha_0 \left[1 + \sum_{i=1}^{p} \alpha_i z^i \right]^{-1} \tag{2b}$$

where the order p is constant and the numerator is such that $\max_{i \geqslant 0} c_\alpha(i) = 1$. The assumption of causality has the simple physical interpretation that the nerve cell is passive. The stability assumption restricts $C_\alpha(z)$ to the region where $0 < |\xi_i| < 1,\ i = 0, \ldots, p-1$, and ensures that the energy flowing through the system is dissipative.

As with any model, the above idealization is likely to present a simplification of the true mechanism giving rise to measured excitatory post-synaptic currents from neuronal cell bodies. For example, in reality the amount of neurotransmitter released may not be strictly proportional to the peak inward current at the synaptic junction [10,11] and the cable properties of the dendrite may only be approximately represented by a time invariant linear filter [12]. Moreover,

there is emerging evidence to suggest that post-synaptic responses may not necessarily be passively relayed to the recording site [13]. Behavioral characteristics of this kind, that call into question the real world authenticity of the assumptions, can be tested for using our methodology and modifications of our basic processing technique that will allow for alternative structures that exhibit such features can also be devised, but we do not pursue the latter avenue here.

The assumption that the additive noise contaminating the post-synaptic current is a zero-mean, white Gaussian process needs to be addressed, however, because real intercellular recordings often exhibit baseline noise that is both skewed, due to spontaneous potentials or currents, and has a colored spectrum. In standard analysis such variation is partly accounted for by measuring amplitudes relative to a baseline in a local neighborhood of the peak. A similar approach can be adopted here by introducing a step function $b(k+(i-1)L) = \beta(i),\ i = 0,\ldots,N-1,\ k = 0,\ldots,L-1,$ that represents the (time varying) baseline associated with the ith stimulus. The baseline function $b(t)$ can be accommodated in practice by using the measurements immediately preceding the onset of the pulse, where the neuron is at rest, to determine the baseline value. This approach corresponds to applying a local time average to estimate each $\beta(i)$ and then conducting the analysis in terms of the corrected response profile rather than the raw data values. It is directly analogous to the nonlinear filtering that is employed with conventional analysis. Alternatively, it is straightforward to incorporate $\beta(i)$, $i = 0,\ldots,N-1$, into the parameter estimation process described in Step 1 below. Although the baseline function $b(t)$ provides a means of dealing with what we might call low frequency baseline wobble and will remove any undesirable non-zero direct-current present in the measurements it will not deal with sources of error, such as amplifier noise, that introduce high frequency noise components. The latter form of noise is more difficult to adjust for and we will provide more detailed discussion of this issue below.

It seems reasonable to conjecture that the model and the associated methodology will be *robust* in that changes in the parameter values will allow the model to adapt to and explain different situations but departures from the underlying assumptions that are not of direct relevance to the scientific question of interest will not seriously degrade its performance. The basic purpose of a model is to help separate the systematic behavior of interest from the background noise and our method is designed to minimize the mean squared error of the discrepancy between the signal deduced from the processing scheme and $s(k)$, the true but unknown signal. Elsewhere we have provided a set of mathematical proofs showing that under appropriate regularity conditions differences between the values estimated from the data and the true values governing the observed process will converge to zero as the number of observations $T = NL$ becomes large (Theorems 3.2, 4.2 and 5.1 of [14]). These and related theorems given in [14] form a theoretical justification for using an

idealized model or approximation when the true complexity of the process is unknown or precludes the formulation of a tractable analytical scheme. In this paper we present empirical evidence that the data processing technique proposed here is indeed *robust* and can be used to detect shortcomings in the model, giving indications of ways in which the specification, and hopefully our understanding of post-synaptic currents, can be improved.

Finally, the adequacy of the model as a description of observed data sequences is illustrated in Fig. 2, where post-synaptic currents recorded from a hippocampal neuron before (upper trace) and after (lower trace) the induction of long-term potentiation are shown. The observed synaptic currents of 20

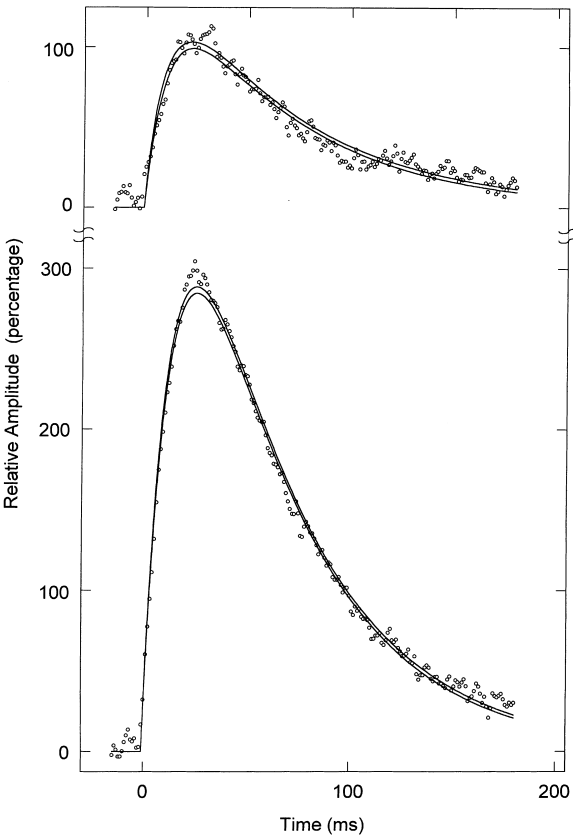

Fig. 2. Synaptic currents recorded from the soma of a hippocampal neuron. Open circles in the upper and lower traces represent, respectively, the averages of 20 evoked responses obtained before and after the induction of long-term potentiation. The data points are fitted with a transfer function, $\alpha(z)\doteq(1-0.982z^{-1})(1-0.925z^{-1})$. The continuous lines represent upper and lower 95% confidence intervals for the impulse response. For details of recordings, see [20,21].

traces are summarized by plotting the averages, shown as open circles. The measured data points are fitted with a transfer function $\alpha(z) \doteq (1 - 0.982z^{-1})(1 - 0.925z^{-1})$ and the lower and upper 95% confidence intervals about the fitted impulse response curves are shown as solid lines. The precision with which the impulse response of the model can be estimated, relative to the variation around the curve caused by the noise component, is clearly illustrated. It is not our purpose here to construct a definitive description of post-synaptic recordings from hippocampal neurons, but we note that there is some evidence to suggest that the use of a simple two parameter model in both cases may not be adequate and a slightly more complex specification might be appropriate. Nevertheless, the ability of the model to approximate the measured responses with a fair degree of accuracy, despite possible shortcomings in the specification, is apparent.

2.2. Analytical steps

A finite algorithm is used to estimate the unknown quantities of interest and involves the following three basic steps:

1. Determine a quasi-maximum likelihood estimate of the parameters that characterise the transfer function and with which the synaptic currents recorded from the cell body are to be modeled.
2. Using the estimated transfer function, deconvolve each response and evaluate the corresponding estimates of the pulse amplitudes (the amount of neurotransmitter released).
3. From the amplitude estimates, construct an estimate of the probability distribution of the quantity of neurotransmitter molecules released using kernel smoothing methods.

Each step is described in further detail in the following sections. Those not interested in the technical rationale may proceed to the validation of the methodology without loss of continuity.

2.2.1. Step 1: Parameter estimation

The unknown quantities to be estimated from the data in addition to the parameter vector $\boldsymbol{\alpha} = (\alpha_1, \ldots, \alpha_p)^{\mathrm{T}}$, where T denotes matrix transposition, are the noise variance σ_n^2 and the unobserved amplitudes $\boldsymbol{a} = (a(0), \ldots, a(N-1))^{\mathrm{T}}$. Assume, temporarily, that the model obtains so that $c_\alpha * u(k) \equiv s(k)$ and $n(k) \equiv \eta(k)$. Utilizing the white Gaussian noise assumption, the joint probability of the observed data given the actually realised but unobserved impulse train heights $\boldsymbol{a}$ and the parameters $\boldsymbol{\alpha}$ and σ_n^2 can be written as

$$\prod_{t=0}^{NL-1} \frac{1}{\sqrt{2\pi\sigma_n^2}} \exp\left(-\frac{1}{2} \frac{n(t)^2}{\sigma_n^2} \right), \tag{3}$$

where $n(t) = y(t) - c_\alpha * u(t)$, $t = 0, \ldots, NL-1$. We seek to maximize Eq. (3) with respect to the unknowns $\boldsymbol{\alpha}$, σ_n^2 and $\boldsymbol{a}$. Given any value for the parameter $\boldsymbol{\alpha}$, $\boldsymbol{\alpha} = \dot{\boldsymbol{\alpha}}$ say, it is easily verified that the optimizing values $\dot{\boldsymbol{a}}$ and $\dot{\sigma}_n^2$ associated with that value are obtained by first solving the equations

$$\dot{a}(i) = \frac{\sum_{j=0}^{L-1} y(iL+j)c_{\dot{\alpha}}(j)}{\sum_{j=0}^{L-1}(c_{\dot{\alpha}}(j))^2}, \quad i = 0, 1, \ldots, N-1, \tag{4}$$

for the amplitudes $\boldsymbol{a}$ and then

$$\dot{\sigma}_n^2 = \frac{1}{NL}\sum_{i=0}^{N-1}\sum_{j=0}^{L-1}(y(iL+j) - \dot{a}(i)c_{\dot{\alpha}}(j))^2, \tag{5}$$

for the variance σ_n^2. Substituting Eqs. (4) and (5) into Eq. (3), taking the logarithm and then negating the result yields

$$\mathscr{L}(\dot{\boldsymbol{\alpha}}) = \frac{NL}{2}\left(\log\left(2\pi\dot{\sigma}_n^2\right) + 1\right). \tag{6}$$

Relaxing the assumption that the model obtains we now treat $\mathscr{L}(\boldsymbol{\alpha})$ as a criterion function for general $\boldsymbol{\alpha}$ that determines our estimate. The minimization of $\mathscr{L}(\boldsymbol{\alpha})$, which we call the *quasi-profile log likelihood function*, generates a value $\hat{\boldsymbol{\alpha}}$ of $\boldsymbol{\alpha}$ called the *Gaussian estimator*. The determination of $\hat{\boldsymbol{\alpha}}$ involves the use of a Newton–Raphson type algorithm, application of which to non-linear statistical problems is documented in [15]. Details of the evaluation of $\hat{\boldsymbol{\alpha}}$ are given in [14].

2.2.2. Step 2: Amplitude deconvolution

The properties of the input process imply the convolution $c_\alpha * u(t)$ takes the values $a(i)c_\alpha(j)$, $j = 0, \ldots, L-1$, in the ith pulse interval, $i = 0, 1, \ldots, N-1$, since by assumption $c_\alpha(i) \approx 0$ for $i \geqslant L$. If we evaluate the impulse response sequence at $\boldsymbol{\alpha} = \hat{\boldsymbol{\alpha}}$ then the residual vector can be written as

$$n(iL+j) = y(iL+j) - a(i)c_{\hat{\alpha}}(j), \quad j = 0, \ldots, L-1, \tag{7}$$

where $a(i)$ denotes the (unknown) pulse height produced by the ith stimulus. The deconvolution that minimizes the residual sum of squares is obviously obtained by regressing the measurements obtained in the ith interval, the observed pulse profile, on the impulse response sequence $c_{\hat{\alpha}}(j)$, $j = 0, \ldots, L-1$. This gives precisely the same values for $\hat{a}(i)$, $i = 0, 1, \ldots, N-1$, as obtained via the Gaussian estimator in Eq. (4) and the residual mean square yields the same noise variance estimate as in Eq. (5).

2.2.3. Step 3: Non-parametric density estimation

Use the amplitude estimates $\hat{a}(i)$, $i = 0, \ldots, N-1$, to determine the amplitude distribution. More specifically, questions of interest concerning $\mathbb{P}_A$ can be addressed by reference to the density estimate

$$\hat{p}_A(a) = (N\beta_N)^{-1} \sum_{i=0}^{N-1} K\Big[(\hat{a}(i) - a)/\beta_N\Big], \tag{8}$$

where $K(\cdot)$ is a basic kernel function such that $K(x) \geqslant 0$, $\int K(x)\,\mathrm{d}x = 1$, and β_N is a bandwidth parameter chosen such that $\beta_N \to 0$ as $N \to \infty$, $N\beta_N \to \infty$. The choice of kernel and the bandwidth parameter is guided by the requirement that the estimate should minimize the asymptotic mean integrated squared error (see [16,17]).

Remark 1. Formulae for the variance–covariances associated with the estimates $\hat{\boldsymbol{\alpha}} = (\hat{\alpha}_1, \ldots, \hat{\alpha}_p)^{\mathrm{T}}$ and $\hat{a}(i)$, $i = 0, 1, \ldots, N-1$, based on Fisher's measure of information, are presented in [14]. These can be readily evaluated as a by-product of the calculations outlined in Steps 1 and 2. Thus we can construct standard errors and test various hypotheses of interest concerning the transmission mechanism. For example, for the post-synaptic currents recorded from a hippocampal neuron employed previously, we find that the null hypothesis $|\xi_i| \geqslant 1$, $i = 0, 1$, is rejected against the alternative $0 < |\xi_i| < 1$, $i = 0, 1$ at the 1% level of significance, implying that there is reasonably strong evidence in favor of a causal, stable transfer function for this data.

Remark 2. Note that Eq. (3) is really a conditional likelihood and the complete likelihood is not available because the probability distribution of the unobserved pulse heights is unknown. Indeed, it is precisely the probability measure $\mathbb{P}_A$ that is the focus of scientific interest and which we wish to ascertain. Once the estimates $\hat{a}(i)$, $i = 0, \ldots, N-1$, have been calculated from the original data they can be taken as noisy observations on the unknown pulse heights and examined directly in order to investigate the nature of the amplitude fluctuations. This might be done using techniques currently in vogue in the quantal analysis of post-synaptic currents that are based on mixture deconvolution with unknown number and type of parent distribution [6]. Given the degree of uncertainty surrounding $\mathbb{P}_A$, however, it seems desirable to impose as little a priori structure as possible. Therefore the approach that we advocate is to use kernel smoothing methods as a basis for making inferences about the amplitude distribution.

Remark 3. It is important to observe that $\hat{p}_A(a)$ is in fact estimating the distribution of the amplitude estimates and the true distribution $\mathbb{P}_A$ will be convolved with that of the errors $\hat{a} - a$ to give the distribution of the $\hat{a}$s. Suppose that it is conjectured that the underlying amplitude distribution $\mathbb{P}_A$ consists of $n_a + 1$ quantal levels with values $a(i)$ and probability of occurrence given by $p_{(i)} = \Pr(a = a(i))$, $i = 0, \ldots, n_a$. As $N \to \infty$ and $L \to \infty$ the errors $\Delta a = \hat{a} - a$ may be treated as zero mean Gaussian random variates with variance

$\sigma^2_{\Delta a} \propto \sigma^2_n/NL$ (see [14]). [2] This implies that $\mathbb{P}_{\hat{A}}$ can be closely approximated by a convolution of Gaussian laws. Thus if $\mathbb{P}_A$ is quantal we can expect $\hat{p}_A(a)$ to resolve into a mixture of n_a normal densities centered at the quantal values $a(i)$ with ordinates proportional to $p_{(i)}$ and common variance proportional to the reciprocal of the product NL. By selecting N and L sufficiently large, therefore, the practitioner can increase the precision with which $\hat{a}$ estimates the unobserved amplitudes and make $\sigma^2_{\Delta a}$ sufficiently small in relation to the quantal separation that the presence of quanta in $\mathbb{P}_A$ will be readily ascertained with little ambiguity by simple visual inspection. Examples that clearly illustrate such behavior are presented below.

Remark 4. There may be cases where it is not clear as to whether the appearance of a local mode (or bump) in $\hat{p}_A(a)$ is a statistical artifact due to sampling fluctuation or is to be attributed to a genuine quantal level. One approach to this problem is to employ the procedures for detecting the number of underlying modes in a distribution suggested by Silverman [16] or a test of the veracity of the assumption of quantal neurotransmitter release can be conducted using the techniques devised by Chu and Chung [18] for detecting jump-discontinuities in distributions. Such methods suppose, however, that the random variables of interest are observed directly and do not make explicit allowance for the pre-processing that takes place in order to construct the amplitude estimates. To overcome this difficulty we have employed bootstrapping techniques similar to the methods used by Stricker et al. [6] in the context of fitting mixture distributions to post-synaptic measurements. Here we employ a semiparametric bootstrap by resampling from the empirical distribution of the $\hat{a}(i),\ i = 0, 1, \ldots, N-1$, $\mathbb{P}_{\hat{A}}(a) = (\{\text{the number of } \hat{a}(i) < a\}/N)$, passing these through the estimated transfer function $C_{\hat{\alpha}}(z)$ to generate the resampled signal, and then adding a random error drawn from $\mathbb{P}_n(\eta)$, the empirical distribution of the fitted residuals. This produces a single bootstrap realization or resample and by repeating this process we can generate bootstrap

[2] Some variance reduction is achieved with traditional methods. Thus, if after baseline correction $2M+1$ values of the post-synaptic current are taken symmetrically balanced around the peak amplitude $a(i)c_\alpha(k_p)$, $c_\alpha(k_p) = \max_{i \geqslant 0} c_\alpha(i)$ then the estimated amplitude is $\bar{a}(i) = (2M+1)^{-1}\sum_{k=-M}^{M} y(k+k_p+(i-1)L) = (2M+1)^{-1}\{a(i)\sum_{k=-M}^{M} c_\alpha(k+k_p) + \sum_{k=-M}^{M} n(k+k_p+(i-1)L)\}$. The variance of this estimate is $\sigma^2_n/(2M+1)$. But the standard error of the $\hat{a}$s will be substantially less than that of the $\bar{a}$s since $NL \gg 2M+1$, the former use the information in all the recordings to estimate each $a(i)$ and not just local information in a neighborhood of a single peak. Note also that, unlike $\hat{a}(i)$, $\bar{a}(i)$ is a biased estimate of $a(i)$ because in general $(2M+1)^{-1}\sum_{k=-M}^{M} c_\alpha(k+k_p) \neq 1$ and the bias $a(i)\{(2M+1)^{-1}\sum_{k=-M}^{M} c_\alpha(k+k_p) - 1\}$ will increase as M is increased.

resamples and construct bootstrapped confidence intervals or hypothesis tests in the usual way, see [19].

3. Validation of the analysis technique

The reliability and the limitations of our methodology were assessed by an extensive simulation study using known signals buried in noise. From the results of these simulations we have ascertained, firstly, that the technique is capable of reliably estimating the underlying pulse shape of the post-synaptic current, even when the amplitude of the individual signal is about the same as the standard deviation of the background noise and the available observation sequence is very short. Secondly, amplitude distributions constructed using the technique closely approximate the actual probability distribution used to generate values of the impulse heights. In particular, the technique correctly deduced whether or not transmitter release occurs in quanta. Thirdly, when the observation sequence was composed of a mixture of large and small post-synaptic currents induced by different release sites, with one located at a more distal segment of the dendrite than the other, it was possible to detect this structure. Finally, whenever small artifactual peaks appeared in the amplitude histogram, which might have led to an erroneous conclusion that the underlying process originated from a mixture of two or more distributions, our testing scheme correctly relegated these deviations to sampling fluctuations.

3.1. Data generation

The fictitious excitatory post-synaptic current data generating mechanisms used in our simulations were structured in such a way that the parameters would approximate those of real signals recorded from the hippocampal pyramidal cell [20,21]. Unless specified otherwise, the signals were generated by passing a series of pulses of differing amplitudes through a transfer function $\alpha(z)^{-1}$, $\alpha(z) = (1 - 0.97z^{-1})(1 - 0.81z^{-1}) = 1 - 1.78z^{-1} + 0.7857z^{-2}$. Hereafter, we will denote the pure, noise-free, signal generated by the parameters of such a transfer function using the compact notation $[1, -1.78, 0.7857] \models s(n)$, which we read as $[\cdot]$ *models* $s(n)$. The length L of each segment was 250 data points and, unless otherwise specified, the observation sequence for each simulation was composed of 1000 such segments. The amplitude of the pulses was varied such that its probability distribution would be either discrete, giving five quantal levels, or continuous. To each signal zero-mean, white, Gaussian noise was added. The amplitude variation of the signals relative to the standard deviation of the noise was varied systematically. To mimic real data, we assumed that the record was filtered at 1 kHz (digitized at 2 kHz) and the

standard deviation of the noise was 1 pA. Throughout we express the amplitude of the signal in pA and the time in ms. These units are arbitrary as far as the methodology is concerned and have only been adopted here in keeping with the real experimental data.

3.2. Identification of quantal distribution

When the amplitude probability distribution of the true signals was quantal, our processing technique correctly deduced that transmitter release occurred in quantum. In contrast, the amplitude histograms constructed using conventional methods of sampling the maximum pulse height merely showed artifactual peaks uncorrelated to the underlying quantal distribution. Indeed, the asymptotic histogram calculated from the convolution of the constituent Gaussian distributions presents a smooth distribution with no discernible peaks.

Figs. 3 and 4 show the results of such simulations. In the data segments illustrated in Figs. 3(A) and 4(A), the underlying signals were, for clarity, arranged such that their amplitudes increased progressively. In the data processed, of course, the signals of different amplitudes and the absence of any signal, representing failures, appeared randomly, their relative frequencies of occurrence being predetermined by the chosen amplitude distribution. The peak amplitude histograms constructed from the data segment containing 1000 evoked post-synaptic responses (including failures) are shown as bar graphs in Figs. 3(B) and 4(B). Superimposed on the bar graphs are mixtures of six Gaussian distributions each with a standard deviation equal to σ_n and with their means located at the different possible amplitude values of the underlying signal. The mixture weights are given by the probabilities associated with each different value. These distributions represent the theoretical asymptotic probability density functions that would be obtained using traditional methods if the location of the peak amplitude were known, (i.e., $M = 0$ and k_p known in footnote 2). The results obtained using the method of analysis outlined in this paper are illustrated in the two last panels of Figs. 3 and 4. The true and estimated impulse responses are depicted in Figs. 3(C) and 4(C), the estimated signals are, respectively, $[1, -1.76, 0.76] \models \hat{s}(n)$ and $[1, -1.76, 0.77] \models \hat{s}(n)$. These estimates are close to those of the true signal, which we recall is $[1, -1.78, 0.7857] \models s(n)$. Using $C_{\hat{s}}(z)$ the estimate of the amplitude of each record was calculated and the underlying amplitude fluctuations in all the evoked signals derived. The distribution functions illustrated in Figs. 3(D) and 4(D) were then obtained from the amplitude estimates using the nonparametric kernel smoothing procedure, as detailed in the previous section. In Fig. 3(D) the upper and lower 95% bootstrap confidence intervals are also shown but for clarity these have been omitted in Fig. 4(D). Superimposed on the probability density curves are the probability mass distributions of the original amplitudes.

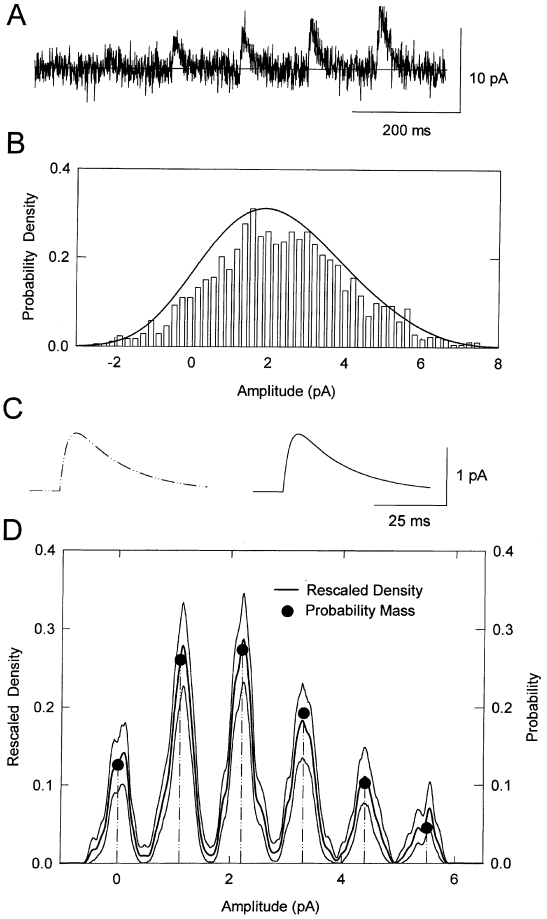

Fig. 3. Low-noise quantal synaptic currents. (A) A segment of 1500-point data containing six traces of evoked records is shown. The duration of each trace was 125 ms. The first of six traces contains no evoked synaptic response. The amplitude of the five subsequent evoked potentials increases progressively from 1.1 to 5.5 pA, in steps of 1.1 pA. Each evoked response was embedded in noise with a standard deviation of 1 pA. (B) The amplitude histogram, shown as a bar graph, was constructed by tabulating the peak value of each evoked potential at a fixed latency. Superimposed on the bar graph is the asymptotic mixture distribution, shown as a continuous line, calculated by adding six Gaussian distributions with appropriate means and variances. (C) The time course of the original signal, the dashed line, is compared with that of the estimated signal, the continuous line. (D) The estimated probability distribution of the pulse heights, the bold solid line, and upper and lower 95% bootstrap confidence intervals, the thin lines, are superimposed on the probability mass distribution of the original signal, shown as filled circles and broken lines. The probability measure of the original signal was obtained from a truncated Poisson distribution of the form $\mathscr{P}_A(a=k) \propto [\exp(-\lambda)\ (\lambda)^k]$, $k = 0, 1, \ldots, 5$, with $\lambda = 2.1$. The synaptic response associated with each realization of the amplitude process was generated by passing the pulse through a second order transfer function, $C_\alpha(z) = \alpha(z)^{-1}$, $\alpha(z) = (1 - 0.97z^{-1})(1 - 0.81z^{-1})$.

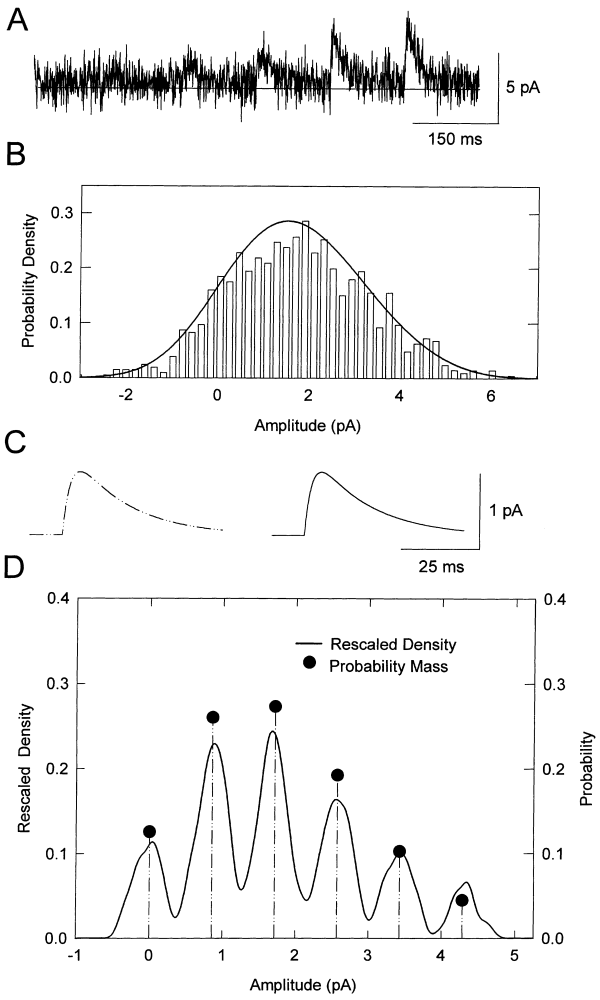

Fig. 4. High-noise quantal synaptic currents. The amplitude of the synaptic current contains five discrete levels increasing progressively from 0.85 to 4.3 pA, in steps of 0.85 pA. See the legend of Fig. 3 for further details.

From a large number of simulation studies such as those illustrated in the previous figures we have ascertained that the technique is capable of extracting the salient features of the data generating mechanism even when the signal-to-noise ratio is further reduced or when the number of quantal levels is increased. The simulation results presented in Fig. 5, for example, demonstrate that the performance of the technique is not impaired when the data sequence contains a large number of discrete signal levels. As in the previous two figures, the four

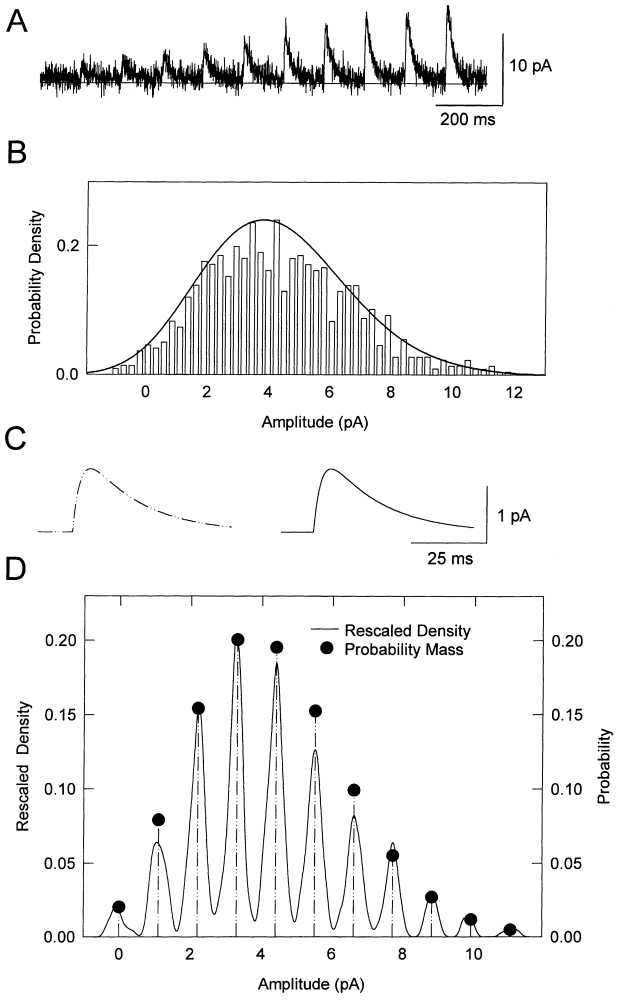

Fig. 5. Synaptic currents with a large number of quantal levels. Synaptic currents with 10 discrete amplitude levels were generated. The probability mass distribution was determined from a truncated Poisson distribution with $\lambda = 3.9$. See the legend of Fig. 3 for detailed particulars.

panels in Fig. 5 show, respectively, (A) segments of the data in which the signals are ordered according to increasing amplitude, (B) the peak amplitude histogram (bar graph) tabulated from the data together with the asymptotic limiting probability density (solid curve), (C) the original signal (broken line) and estimated signal (solid line) from the observation sequence, and (D) the estimated amplitude distribution (continuous line) and the probability mass distribution of the original signal (filled circles and broken lines).

In the previous series of simulations, the number of records in the data was kept constant at 1000. To ascertain how much data are required to obtain a reliable estimate of the true amplitude distribution we have systematically reduced the value of N. In Fig. 6 the estimated amplitude distributions obtained from three simulations are exhibited. The number of records contained in the three data sets were 250, 100 and 50 in Figs. 6(A), (B) and (C), respectively. Obviously, the parameter estimates become less accurate as the data length is

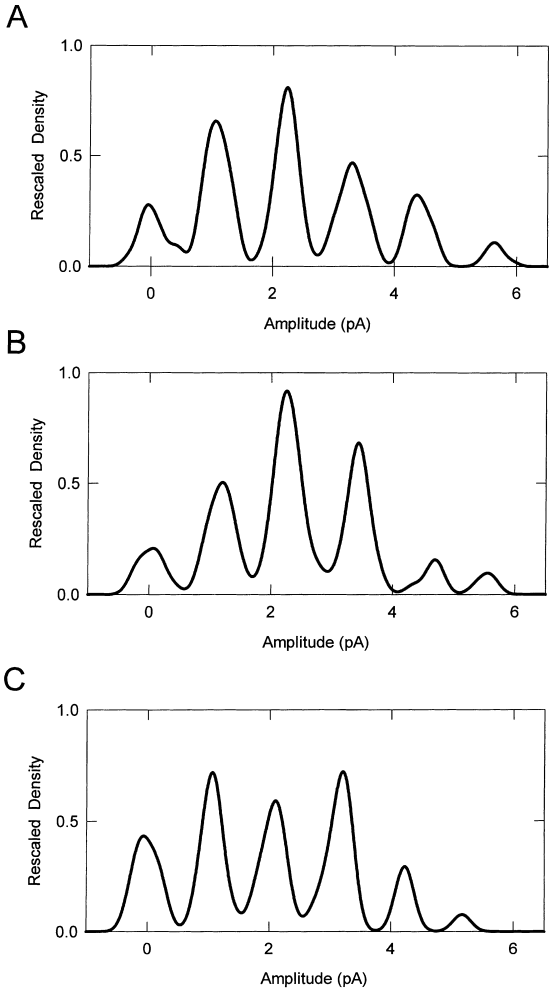

Fig. 6. Sensitivity to decreasing data length. Three amplitude density estimates were calculated from different data segments containing (A) 250, (B) 100 and (C) 50 traces of 125 ms. The parameters used to generate the data were identical to those employed in Fig. 3.

decreased but the estimated signal did not deviate appreciably from the true value even when the number of records in the data was only 50. The estimated parameters of the signal were $[1.0, -1.78, 0.78]$ with 250 records, $[1.0, -1.73, 0.74]$ with 100 records, and $[1.0, -1.78, 0.87]$ with 50 records. The estimated amplitude distributions clearly reflect the underlying structure of the true data generating mechanism even at these relatively small sample sizes.

3.3. Quantal variation and different release sites

Generally, the amplitudes of evoked synaptic currents at central synapses fluctuate from a mean quantal level. Also, the release sites may be located at different dendritic segments, some forming synaptic contacts at more distal sites than others. The presence of these factors, that will tend to obscure quantal peaks, can readily be ascertained by applying the analytical scheme we propose here.

The two data records displayed in Fig. 7(A) were generated to mimic a situation in which the measured currents originate from two release sites, one located near the soma and the other further away. The modal amplitudes of the two signals were 2 and 3.8 pA, giving an overall amplitude of 5.8 pA for the signal resulting from the coincidental release from both sites. The synaptic response from the more distal release site was more heavily filtered than that from the proximal release site (Fig. 7(A), upper trace), although once buried in the noise the differences in the time profile of the three responses are visually indiscernible (see Fig. 7(A), lower trace). The amplitude histogram constructed by sampling peak points from each record would ultimately give rise to the algebraic sum of four Gaussian curves, as shown in Fig. 7(B). For the particular amplitude distribution we used to generate the data, this produces a skewed curve centered near the 0 pA level with a subsidiary peak located near the 4 pA level. However, the amplitude probability density curve derived by using our technique under the erroneous assumption that the parameters of all the signals contained in the observation sequence are identical reveals four clear peaks, representing baseline noise (failures) and three post-synaptic current levels (Fig. 7(C)). With the knowledge that the evoked synaptic currents had four distinct amplitudes the various records containing the different responses were separated into four groups, representing failures, local release, distant release and simultaneous release, respectively. The parameters of the signal in each group were then estimated separately. In Fig. 7(D), the estimated signals (continuous lines) are superimposed on the original signals (broken lines). The estimated parameters of the two signals were, $[1.0, -1.83, 0.83] \models \hat{s}_1(n)$ and $[1.0, -1.32, 0.34] \models \hat{s}_2(n)$, compared to the corresponding true parameter values of $[1.0, -1.78, 0.79] \models s_1(n)$ and $[1.0, -1.34, 0.36] \models s_2(n)$. We note here that the separation of the events will not be reliable if synaptic currents emanating from the two synaptic sites are not of different amplitudes. Jack et al. [3], among

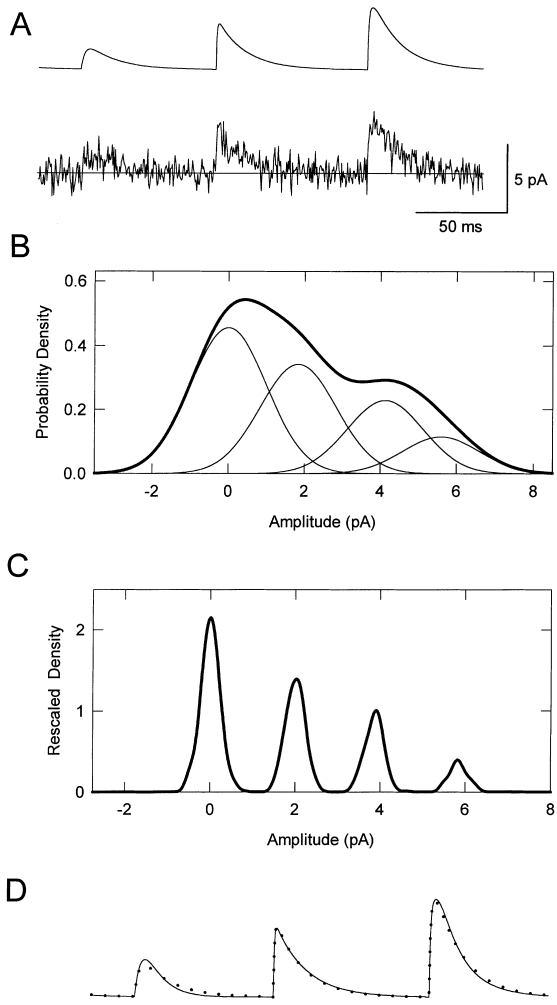

Fig. 7. Synaptic currents originating from two different release sites. (A) Three evoked responses in the absence (upper record) and presence (lower record) of measurement noise (with $\sigma_w = 1$ pA) are displayed. The amplitudes of the synaptic currents generated from the two release sites were 2 and 3.8 pA, a third observed synaptic response results from a coincidental activation of both release sites. (B) The finite mixture distribution (heavy line) arising from the sum of four Gaussian distributions (light lines) reveals two broad peaks. (C) The amplitude histogram of pulse heights estimated from the data. (D) The time-course of each of three synaptic responses contained in the record was estimated (solid line), and superimposed on that of the true signals used to generated the data (broken line).

others, have shown that synaptic potentials arising from different dendritic locations in the spinal cord can have similar amplitudes.

It is known that the amplitude of the spontaneous miniature post-synaptic potentials in the neuromuscular junction fluctuates around modal values with a coefficient of variation ranging from 0.1 to 0.3. The coefficient of variation equals the ratio of the standard deviation of a distribution to its mean [22]. Although direct determinations of this value in central neurons are difficult to make one recent study based on the observed amplitudes of spontaneous miniature currents using whole cell recording suggests that the coefficient of variation may be as large as 0.4–0.6 [23]. Theoretically, a peak amplitude histogram constructed from post-synaptic currents generated by a multi-modal amplitude distribution with a coefficient of variation in the region of 0.5 will in the limit appear as a continuous unimodal distribution, even in the absence of additive noise and measurement errors. Our simulations reveal that provided the coefficient of variation does not exceed 0.4 and the modal quantal levels are separated from each other by about 3 standard deviations of the background noise then the individual quantal peaks and the baseline can be revealed clearly using our analytical method.

The results of two such simulations are illustrated in Figs. 8 and 9. The top traces, Figs. 8(A) and 9(A), are segments of noise-contaminated post-synaptic currents based on amplitude values drawn from the probability density functions shown in Figs. 8(B) and 9(B). These distributions are derived by assuming three equally likely modal values occur at 1, 2 and 3 pA, with the probability of failure taken to be 0.2. In Fig. 8(B) the convolution of this distribution with a Gaussian density possessing a coefficient of variation of 0.3, representing the quantal variation, is given and Fig. 9(B) depicts the equivalent theoretical amplitude probability density when the coefficient of variation is 0.4. In the absence of noise the three modes corresponding to the three basic quantal levels can be discerned. When background noise with a standard deviation of 0.4 and 0.3 pA, respectively, is added, however, the peaks are virtually obscured in the theoretical asymptotic probability density functions, as shown in Figs. 8(C) and 9(C). From Figs. 8(D) and 9(D), however, we see that the amplitude distributions derived using our method recover the original modes reasonably clearly, the measurement noise notwithstanding. By deconvolving the estimated distribution into the constituent normal densities the underlying coefficients of variation can be readily recovered. The estimated signals in these two simulations were $[1.0, -1.78, 0.79] \models \hat{s}(n)$ and $[1.0, -1.78, 0.78] \models \hat{s}(n)$ for the results illustrated in Figs. 8 and 9, respectively.

3.4. Continuous amplitude distribution

It is possible that the amplitude distribution of post-synaptic currents recorded from neurons in the brain, unlike those from neuromuscular junctions,

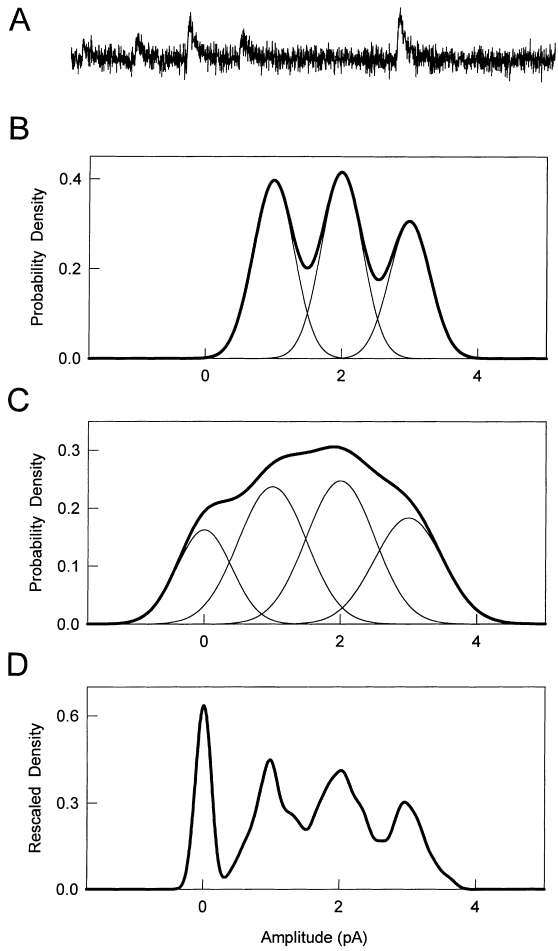

Fig. 8. Synaptic currents with a small quantal variation. (a) Pulses of various heights were sampled randomly from the probability density in (B) and then a synaptic response associated with each realised amplitude was generated by passing it through the transfer function given in the legend of Fig. 3. Gaussian noise with a standard deviation of 0.4 pA was added to the signal. The data segment contains five non-zero synaptic responses and two failures. (B) The theoretical amplitude distribution. The three normal curves, shown as light lines, depict the amplitude fluctuations of the synaptic response from the mean/modal value with a coefficient of variation of 0.3. The associated Gaussian convolution generates the mixture distribution, shown as the heavy line. (C) A mixture of four Gaussian distributions, the heavy line, giving the theoretical asymptotic probability density function. The variance of each constituent distribution, represented by light lines, is obtained by adding the variance of the amplitude distribution to that of the noise. (D) The distribution of pulse heights derived from an analysis of the data using the current methodology.

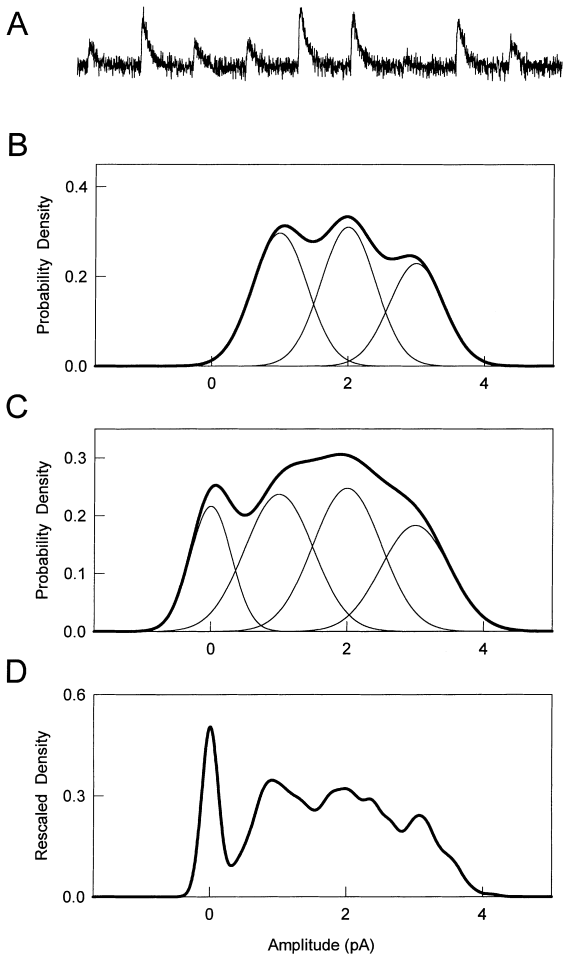

Fig. 9. Synaptic currents with a large quantal variation. The coefficient of variation of the amplitude process was 0.4 whereas the standard deviation of the noise was 0.3 pA. See the legend of Fig. 8 for detailed particulars of the illustrations.

may not show distinct quantal levels. This might be due to the presence of a large number of release sites, large quantal variation in the synaptic terminal or disparate synaptic locations along the dendritic tree [24]. To mimic such behavior we have generated a set of fictitious synaptic currents in which the amplitude probability distribution is given by a mixed mass-density function.

In Fig. 10 the result of one set of such simulations is illustrated. Six examples of the evoked synaptic currents, arranged in order of increasing amplitude, before and after the addition of noise, are shown in Fig. 10(A). The amplitude

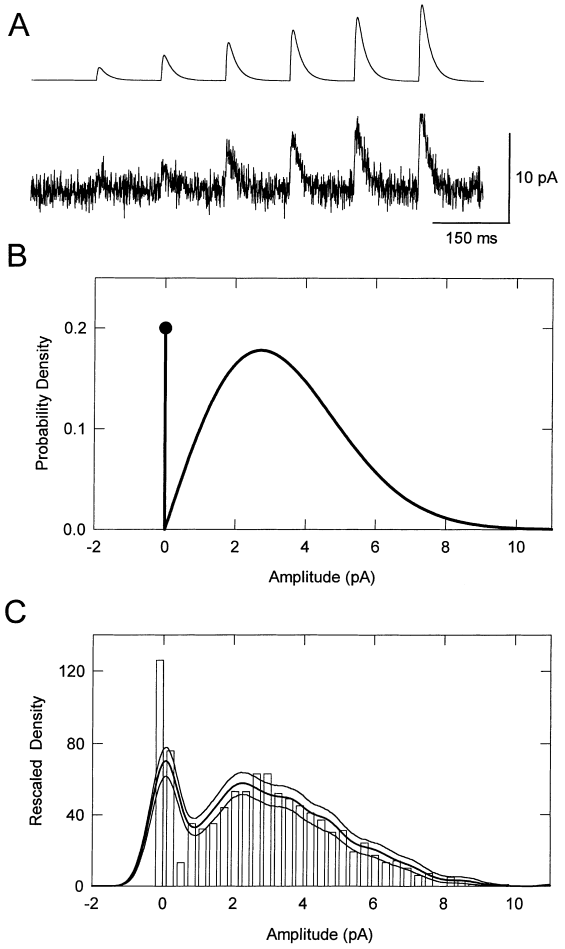

Fig. 10. Continuous amplitude distribution. (A) Two traces illustrating segments of records containing six evoked synaptic currents before (upper trace) and after (lower trace) the addition of Gaussian noise with $\sigma_n = 1$ pA. (B) The amplitude values were randomly selected from the probability distribution function $\mathscr{P}_A(a(i) \leqslant a) = 0.8[1 - \exp(-a^2)]$, $a > 0$, and $\mathscr{P}_A(a(i) = 0) = 0.2$. (C) The distribution of the estimated pulse heights calculated from the data, the bar graph, with the estimated amplitude density function, the bold solid line, and the upper and lower 95% bootstrap confidence intervals, shown as the thin solid lines, superimposed.

of each signal was determined from the probability distribution function illustrated in Fig. 10(B). In Fig. 10(C) the histogram of the amplitude estimates $\hat{a}(i),\ i = 0, 1, \ldots, N-1$, derived from the observed data is shown. For comparison, the estimated density function is superimposed on the bar graph, as are the upper and lower 95% bootstrap confidence intervals. This figure should

be contrasted with Fig. 3. The ability of the processing technique to detect the underlying structure of the data generating mechanism can be clearly seen from the close proximity of the bar graph and the estimated density functions to the theoretical curve.

3.5. Correlated noise

In experimental situations the noise that corrupts the signal is generally not white. We have already noted that the baseline function $b(t)$ provides a means of dealing with low frequency baseline wobble and will remove any undesirable nonzero direct-current present in the measurements. High frequency noise components, such as amplifier noise and background hiss, however, are more difficult to adjust for. From a number of simulations we have ascertained that our method is effective in deducing the structure of the underlying process even when the noise is not strictly white and the technique is quite *robust* to violations of this assumption. One example of such simulations is illustrated here.

The colored noise is obtained by passing white Gaussian noise through a second-order auto-regressive filter whose poles are located at $-0.7 + 0.1\mathrm{j}$ and $-0.7 - 0.1\mathrm{j}$ (where $\mathrm{j} = \sqrt{-1}$). The output of the filter is scaled to produce the desired standard deviation. The power spectrum of the noise, illustrated in Fig. 11A, increases steeply at high frequencies. Using this colored noise, we repeated the simulations illustrated in Fig. 4. Synaptic currents of five discrete peak amplitudes were buried in the colored noise and then the probability distribution of the pulse heights was estimated with our analytical scheme. The shape of the estimated signal (continuous line in Fig. 11(B)) closely matches that of the original signal (broken line in Fig. 11(B)). Also, the estimated amplitudes of the synaptic currents and their relative probability of occurrence are in close agreement with the true values (Fig. 11(C)). We thus conclude that the method we propose here can accurately detect and characterize synaptic currents even when the noise is not white but exhibits characteristics more in accordance with those found in laboratory measurements.

4. Discussion

Amplitude distributions derived by sampling the peak amplitude of evoked endplate potentials reveal that release occurs in quanta. A statistical model developed by del Castillo and Katz [1] to characterize such amplitude histograms relies on the fact that the measurement noise is negligibly small compared to the signal. The synaptic currents recorded from the soma of a neuron, however, are severely filtered and attenuated and also heavily contaminated by noise. Thus it is difficult to draw clear inferences about the nature of the generating mechanism from a peak amplitude histogram derived from such

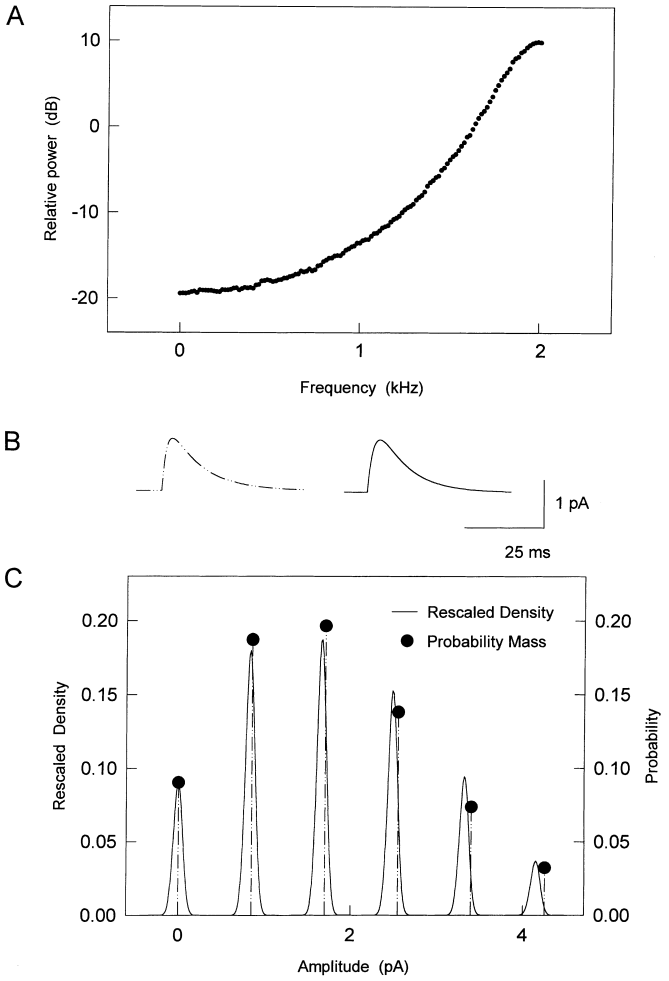

Fig. 11. Synaptic currents embedded in correlated noise. Using colored noise, instead of white noise, the simulations detailed in Fig. 4 were repeated. (A) The power spectrum of the generated noise was calculated by using Welch's averaged periodgram method. (B) The time course of the original signal (broken line) embedded in the colored noise and that of the estimated signal (continuous line) are shown. (C) The estimated probability distribution of pulse heights (continuous line) is superimposed on the probability mass distribution of the original signal (filled circles and broken vertical lines).

data. Moreover, when the number of release sites and/or the quantal variation is very large, a histogram drawn from such a process will ultimately appear as a continuous distribution, although artifactual, poorly resolved peaks may appear owing to random sampling fluctuation. Nevertheless, it is of considerable

importance to be able to determine if the synaptic transmitter in axon terminals is released in the form of packets as in the neuromuscular junction. If it is, it would be helpful to know the magnitude of the quantal content, whether or not quantal peaks are evenly spaced, the number of release sites, and how large the coefficient of variation is. With the analytical scheme presented here we have made it possible to resolve in an unambiguous manner many of these issues concerning the generating mechanisms underlying synaptic transmission in the central nervous system.

The ability of the processing method to extract the salient features of the underlying synaptic transmission mechanism from a limited set of imperfect, noisy measurements is demonstrated in our simulation studies. Using our method we could clearly determine quantal peaks and the quantal content when release did indeed occur in quanta, even when the signal-to-noise ratio was relatively low (Fig. 4), many release sites were present (Fig. 5), and quantal variance was large (Figs. 8 and 9). By examining the parameters of the pulses it was also possible to deduce the synaptic locations relative to the recording site of two different inputs (Fig. 7).

It is possible that, due to a variety of reasons already alluded to, the amplitude of the synaptic currents recorded from neuronal cell bodies of central neurons may be continuously variable. For example, it has been argued that the quantal variance in central neurons is large enough to completely obscure the peaks in the synaptic amplitude histogram of a central neuron [25,26]. The technique described here will correctly identify the underlying amplitude distribution as continuous if there are no quantal synaptic responses (Fig. 10). However, a histogram obtained by selecting a few peak values from each response invariably shows spurious peaks for such an underlying process, especially when the sample size is small and the signal-to-noise ratio is low. Using our processing method, we can test, as described in Remark 4, whether some observed peaks in the amplitude histogram arise from the genuine underlying quantal content or they merely reflect sampling fluctuations and thus should be relegated to statistical artifacts.

The comparisons between the actual and estimated parameter values illustrated in our simulation studies demonstrate that some of the underlying characteristics of the evoked synaptic currents that would have been difficult to obtain using conventional techniques can be extracted with the aid of our analytical scheme. The amplitude distribution obtained by using our method utilizes the information contained in the entire signal sequence, unlike the conventional histogram tabulated from series of peak values taken from each synaptic response. Moreover, the estimated parameters of the signal provide further insight into the underlying data generating mechanism. For example, if the amplitude of evoked synaptic currents increases after a certain experimental maneuvre then it is important to compare the structure of the optimal overall transfer function of the signals before and after the induction of

potentiation. Such information, together with the amplitude probability distribution function derived after the noise corrupted data has been cleansed, may enable us to discriminate between different speculations concerning the basis for long-term potentiation and delineate the more plausible explanations.

Because the acquisition of experimental records containing evoked synaptic currents from in vitro brain preparations is both laborious and technically demanding, analytical techniques that fully exploit the information contained in the data need to be employed. It is with this aim in mind that we propose here one such technique, based on the utilization of modern signal processing methods. This may help elucidate some of the unsolved issues in synaptic transmissions in central neurons, issues that are of fundamental importance in neurobiology.

Acknowledgements

A MATLAB code for implementing the analytical method described here is available upon request. This work was supported by grants from the Australian Research Council and the National Health and Medical Research Council of Australia. We wish to thank Professor Steve Redman and Dr Christian Stricker for allowing us to use their unpublished synaptic current recordings obtained before and after the induction of LTP in hippocampal pathways, which are illustrated in Fig. 2.

References

[1] J. del Castillo, B. Katz, Quantal components of the end-plate potential, J. Physiol. 124 (1954) 560.
[2] I.A. Boyd, A.R. Martin, The end-plate potential in mammalian muscle, J. Physiol. 132 (1956) 74.
[3] J.J.B. Jack, S.J. Redman, K. Wong, The components of synaptic potentials evoked in cat spinal motoneurones by impulses in single group Ia afferents, J. Physiol. 321 (1981) 65.
[4] R.J. Sayer, S.J. Redman, P. Andersen, Amplitude fluctuations in small EPSPs recorded from CA1 pyramidal cells in the guinea pig hippocampal slice, J. Neurosci. 9 (1989) 840.
[5] R.J. Sayer, M.J. Friedlander, S.J. Redman, The time course and amplitude of EPSPs evoked at synapses between pairs of CA3/CA1 neurons in the hippocampal slice, J. Neurosci. 10 (1990) 826.
[6] C. Stricker, S. Redman, Statistical models of synaptic transmission evaluated using the expectation–maximization algorithm, Biophys. J. (1994) 656.
[7] C. Stricker, S. Redman, D. Daley, Statistical analysis of synaptic transmission: model discrimination and confidence limit, Biophys. J. 67 (1994) 532.
[8] D. Liao, A. Jones, R. Malinow, Direct measurement of quantal changes underlying long-term potentiation in CA1 hippocampus, Neuron. 9 (1992) 1089.
[9] T.V.P. Bliss, G.L. Collingridge, A synaptic model of memory: long-term potentiation in the hippocampus, Nature 361 (1993) 31.

[10] V.V. Uteshev, P.S. Pennefather, Analytical description of the activation of multi-state receptors by continuous neurotransmitter signal at brain synapses, Biophys. J. 72 (1997) 1127.
[11] L.M. Wahl, J.B. Jack, A.U. Larkman, K.J. Stratford, The effects of synaptic noise on measurements of evoked excitatory synaptic response amplitude, Biophys. J. 73 (1997) 205.
[12] R. Yuste, W. Denk, Dendritic spines as basic functional units of neuronal integration, Nature 375 (1995) 628.
[13] J. Magee, D. Hoffman, C. Colbert, D. Johnston, Electrical and calcium signaling in dendrites of hippocampal pyramidal neurons, Ann. Rev. Physiol. 60 (1998) 327.
[14] D.S. Poskitt, K. Doğançay, S.H. Chung, Double blind deconvolution: the analysis of post-synaptic currents in nerve cells, J. Roy. Statist. Soc. 61 (1999) 191.
[15] Y. Bard, Nonlinear Parameter Estimation, Academic Press, New York, 1974.
[16] B.W. Silverman, Density Estimation for Statistical Data Analysis, Chapman and Hall, London, 1986.
[17] M.P. Wand, M.C. Jones, Kernel Smoothing, Chapman and Hall, London, 1995.
[18] C.K. Chu, P.E. Chung, Estimation of jump points and jump values of a density function, Statistica Sinica 6 (1996) 75.
[19] B. Efron, R. Tibshirani, An Introduction to the Bootstrap, Chapman and Hall, New York, 1993.
[20] C. Stricker, A.C. Field, S.J. Redman, Statistical analysis of amplitude fluctuations in EPSCs evoked in rat CA1 pyramidal neurons in vitro, J. Physiol. 490 (1996a) 419.
[21] C. Stricker, A.C. Field, S.J. Redman, Changes in quantal parameters of EPSPs in rat CA1 neurones in vitro after the induction of long-term potentiation, J. Physiol. 490 (1996b) 443.
[22] E.M. McLachlan, The statistics of transmitter release at chemical synapses, Int. Rev. Physiol. Neurophysiol. III 17 (1978) 49.
[23] J.M. Bekkers, G.G. Richerson, C.F. Stevens, Origin of variability in quantal size in cultured hippocampal neurons and hippocampal slices, Proc. Nat. Acad. Sci. U.S.A. 87 (1990) 5359.
[24] J.M. Bekkers, Quantal analysis of synaptic transmission in the central nervous system, Current Opinions in Neurobiol. 4 (1994) 360.
[25] J.M. Bekkers, C.F. Stevens, Quantal analysis of EPSCs recorded from small numbers of synapses in hippocampal cultures, J. Neurophysiol. 73 (1995) 1145.
[26] J.D. Clements, Quantal synaptic transmission? Nature 353 (1991) 396.